Bulletin of the Seismological Society of America, Vol. 95, No. 6, pp. 2162–2179, December 2005, doi: 10.1785/0120050047

Bulk Sediment Q_p and Q_s in the Mississippi Embayment, Central United States

by Charles A. Langston, Paul Bodin, Christine Powell, Mitch Withers, Steve Horton, and Walter Mooney

Abstract We have estimated *P*-wave and *S*-wave anelastic attenuation coefficients for the thick, unconsolidated sediments of the Mississippi embayment, central United States, using the spectral distance decay of explosion *P* and Rayleigh waves. The sediment-trapped *P* wave, P_{sed}, is observed to ranges of 80 km at 10 Hz, and 1-Hz Rayleigh waves are observed out to 130 km from a 5000-lb borehole explosion in the northern part of the embayment. Rayleigh waves of 4 Hz are seen to distances of 3 km from a smaller 50-lb explosion. Analysis of the group velocity and amplitude-distance decay of both waves yields an average Q_s of 100 and Q_p of 200 for embayment sediments that are independent of frequency. Scatter in the *Q* estimates comes from interference of multiple *P*-wave reverberations and Rayleigh-wave modes. The attenuation model is self-consistent in that it is the same as obtained by the analysis of synthetic seismograms using the inferred *Q*-values. Inferred Q_p and Q_s values are more than three times higher than previous estimates and imply that unconsolidated sediments of the embayment do not significantly attenuate small-strain earthquake ground motions. These estimates represent a lower bound to *Q* of the sediments since significant scattering is observed in the waveform data that contributes to the distance decay of wave amplitude. Higher *Q* values also imply that the unconsolidated sediments of the embayment will form an efficient wave guide for surface waves radiated from shallow earthquakes or large earthquakes that rupture into the sediments, producing high-amplitude, long-duration wave trains that should be considered in earthquake hazard assessments.

Introduction

The effect of site conditions is a major issue in evaluating the hazards due to strong ground shaking in large earthquakes. Numerous studies have noted both the amplification and attenuation effects of deep, unconsolidated sediments on earthquake ground motions (e.g., see Aki, [1988] for an historical review). Conventional seismological wisdom suggests that the large observed decrease in seismic impedance of unconsolidated sediments relative to underlying basement rocks serves to significantly amplify a vertically propagating shear wave. On the other hand, there are suggestions from strong-motion observations that sediments can significantly attenuate high-frequency body waves because of large intrinsic attenuation. Such large intrinsic attenuation may be a property of porous, fluid-filled unconsolidated media or may be a natural consequence of nonlinear, strain-dependent degradation of the shear modulus at high seismic strains (Vucetic, 1994).

These issues are particularly important for a large area in the central United States surrounding the New Madrid Seismic Zone (NMSZ). The NMSZ is an area of high seismic hazard based on historical accounts of the 1811–1812 seismic sequence (Nuttli, 1973; Johnston and Schweig, 1996) and the geological evidence suggesting the occurrence of large magnitude earthquakes with a recurrence interval of approximately 500 years (Kelson *et al.*, 1996; Tuttle and Schweig, 1999; Tuttle *et al.*, 2000). Compounding the problem of an active source zone is the near-surface geological structure. The NMSZ is blanketed with a thick layer of upper Cretaceous to Recent unconsolidated sediments that are as thick as 1 km under the metropolitan area of Memphis, Tennessee (Stearns, 1957; Stearns and Marcher, 1962; Self, 1993). A number of empirical studies have suggested that these sediments have a significant amplification effect on seismic waves propagating up through them (e.g., Bodin and Horton, 1999; Bodin *et al.*, 2001; Langston, 2003a). Yet, other studies suggest that the unconsolidated sediments are highly attenuating for high-frequency seismic waves. Bulk sediment anelasticity determined in several studies of earthquake *P*- and *S*-wave spectra from 2 to 25 Hz is quite significant with Q_s values ranging from 25 to 40 and Q_p values

ranging from 25 to 60 (e.g., Liu *et al.* 1994; Chen *et al.* 1994). Local geotechnical determinations involving analysis of refracted wave pulse widths yield small values of 10–30 for Q_s for the upper 30 m of the sediments (Wang *et al.*, 1994) and recent VSP results have yielded 22–34 for Q_s for the upper 60 m (Pujol *et al.*, 2002). These geotechnical studies analyzed controlled source shear-wave data in frequency bands above 25 Hz. Other common engineering attenuation models suggest that bulk Q_s values may be as low as 10 based on spectral analysis of local earthquake (small strain) data in the embayment (Hashash and Park, 2001; Park, 2003). Such low Q_s values may attenuate 5-Hz shear waves by as much as 40% or more as they propagate up through the sediments, completely counteracting wave amplification due to the decrease in seismic impedance.

Recently, Langston (2003a,b) showed that the *Sp*/*S* spectral method, the basis of many of the previous Q_s and Q_p estimates, is actually insensitive to anelasticity because of significant near-surface site resonance effects. There are no measurements of Q_s or Q_p for the entire unconsolidated sedimentary column in the embayment that are independent of major biasing assumptions on the propagation of seismic body waves.

The purpose of this article is to present a method and results for determining the bulk Q_s and Q_p for thick sediments based on the analysis of Rayleigh waves and *P* waves generated by large controlled source explosions. This method capitalizes on the fact that unconsolidated sediments have very low wave velocities so that observation of high frequency *P* or Rayleigh waves at large distances greatly constrains the average attenuation of the structure. We will use observations of the trapped sedimentary *P* wave, P_{sed}, to place strong constraints on Q_p in the frequency band of 3 to 10 Hz and observations of 0.4- to 4-Hz Rayleigh waves to place equally strong constraints on Q_s. The method is loosely based on a standard seismological technique for determining the distance attenuation of fundamental mode Rayleigh waves that is routinely used for long-period earthquake data interpretation (Aki and Richards, 1980) and occasionally used for site-specific studies (e.g., Barker and Stevens, 1983). However, we use large explosions detonated within the Mississippi embayment to create high frequency Rayleigh waves and use the redundancy of data available from many permanent and temporary stations at various distances from the source to determine the average distance attenuation coefficient. The measured group velocities and distance attenuation coefficients with standard errors are then used to solve for bulk Q_s^{-1} and Q_p^{-1} attenuation.

The physical interpretation of attenuation measurements is an important issue to be addressed in this work. The empirical measurement of apparent anelastic attenuation of a particular wave always depends on the wave propagation model for the wave. For both *P* and Raleigh waves we will be using very simple assumptions related to mode and ray theory. However, anelastic attenuation should be a seismological material property of earth structure much like *P*-wave or *S*-wave velocity. Empirical attenuation values will be modeled using simple layered anelastic velocity models for the embayment sediments. Synthetic seismograms will be computed and processed in the same manner as the data as a self-consistency check on the empirically derived attenuation values.

We will show that attenuation for the entire sedimentary column is considerably less (i.e., higher Q_p and Q_s) than has generally been assumed. This has important implications for seismic hazards studies and for seismic hazards in the NMSZ.

The Embayment Seismic Excitation Experiment (ESEE)

Our study (ESEE) was a joint experiment conducted by the Center for Earthquake Research and Information (CERI) at the University of Memphis and the Active Source Group at the U.S. Geological Survey (USGS), Menlo Park, California (Langston *et al.*, 2002a). The experiment consisted of the detonation of chemical explosives emplaced in the lower 30 m of 50-m-deep, 20.3-cm (8-in.) steel-cased boreholes. Two sources were employed. On the night of 29 October 2002, a 1134 kg (2500 lb) single borehole explosion was detonated near Mark Tree, Arkansas (Fig. 1). The next night a 2268 kg (5000 lb), simultaneous two-borehole explosion was detonated near Mooring, Tennessee, near the center of the NMSZ. Table 1 contains the pertinent source parameters for the explosions. The smaller explosion had an estimated local magnitude (M_L) of 2.8, as recorded by stations of the cooperative New Madrid network, and the larger explosion was seen to be equivalent to an M_L 3.1. The geometry and style of the experiment was similar to refraction experiments performed by the USGS in the 1980s and early 1990s within the NMSZ (Ginzberg *et al.*, 1983; Mooney *et al.*, 1983; Catchings, 1999).

Unlike past refraction experiments, however, the purpose of the ESEE was to generate seismic Rayleigh waves that could be used to estimate the anelastic attenuation of the unconsolidated embayment sediments. Rayleigh waves were observed from the earlier USGS refraction experiments, and an initial analysis of velocity and attenuation structure suggested that amplitudes for 0.3- to 5-Hz Rayleigh waves should be quite sensitive to anelastic attenuation in the thick low-velocity embayment sediments. The ESEE explosions were recorded by approximately 90 short-period and 12 broadband stations of the cooperative New Madrid seismic network and by 9 additional temporary broadband stations that were deployed to fill in the permanent broadband network. Each explosion was also monitored by a three-component K2 accelerograph positioned approximately 80 m from the shotpoint and by a linear array of 8 three-component K2 accelerographs situated 2.6 km from the Marked Tree source and 1.2 km from the Mooring explosion. Strong motion data from the accelerographs will be treated in a companion report. Here we concentrate on the analysis of the far-field broadband data to derive the ampli-

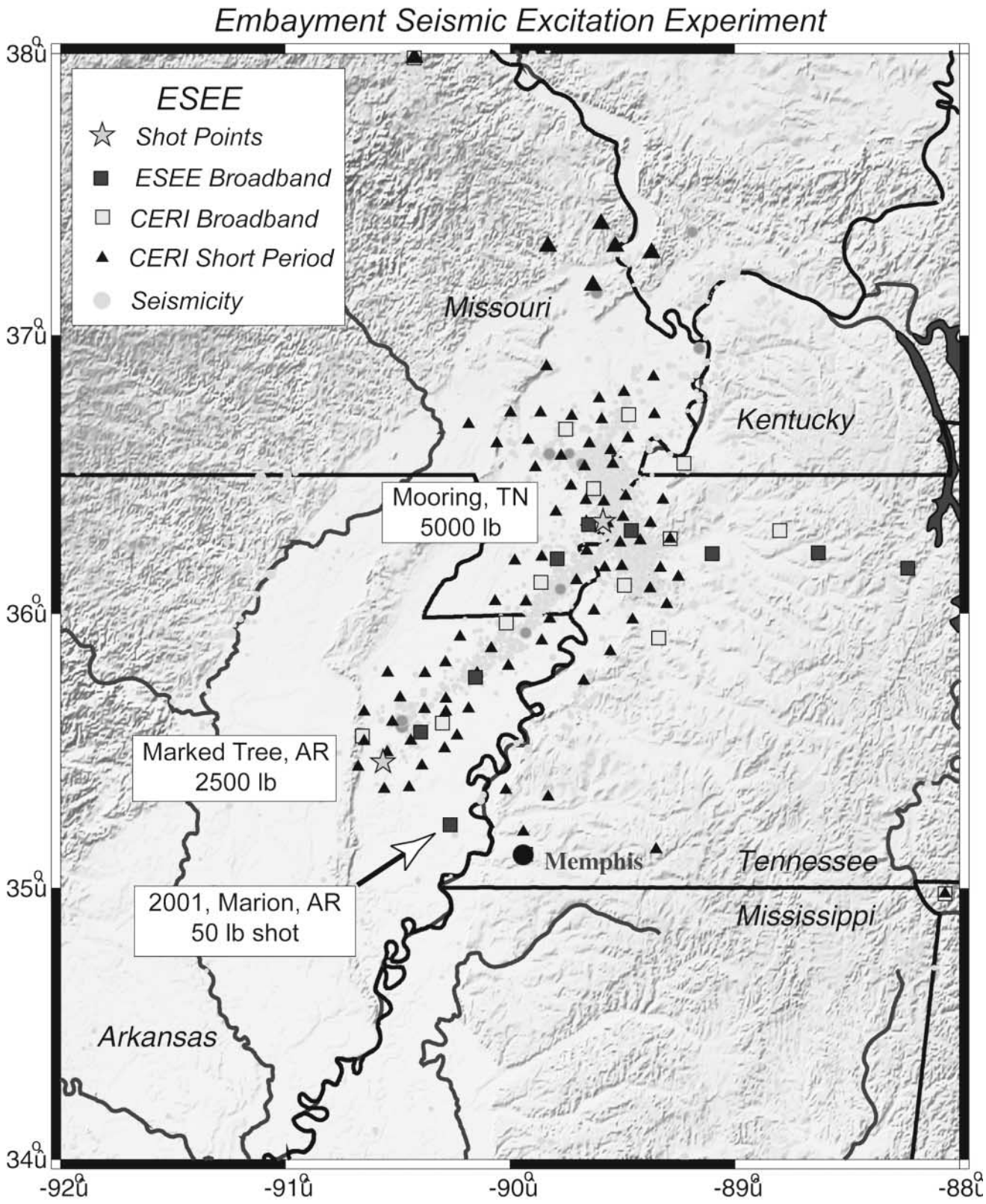

Figure 1

Figure 1. Index map of the New Madrid Seismic Zone in the central United States showing political boundaries, shaded topographic relief, CERI short-period seismic stations (closed triangles), CERI broadband seismic stations (open squares), and temporary broadband seismic stations (closed squares). Shot points for the ESEE explosions are shown as stars and are annotated. Earthquakes of the NMSZ are plotted as gray circles. ESEE was designed to explore the effects of sediment velocity and attenuation structure within the NMSZ.

tude-distance decay of Rayleigh waves and the trapped P_{sed} wave that are confined to the unconsolidated sediments.

Examples of these waves are shown in Figure 2. P_{sed} is best seen in the 3- to 10-Hz frequency band and consists of multiple turning waves and reflections from the base of the unconsolidated sediments. It has a characteristic group velocity of 1.8 to 2.0 km/sec, is generally larger than first arriving refraction *P*-wave phases, and has been observed in past refraction experiments in the area (e.g., Mooney *et al.*, 1983). Rayleigh waves show normal dispersion and are largest in the 1- to 2-Hz frequency band. Rayleigh waves from the 5000-lb explosion were detected at 130-km distance within the embayment. Figure 3 shows a constructed pseudo-profile of filtered vertical displacement data. Short-period embayment Rayleigh waves travel at group velocities of 250–500 m/sec causing surprisingly long-duration wave trains.

Marion, AR, Test Explosion

Rayleigh wave data from a small 23-kg (50-1b) chemical explosion were collected in April 2001 for an irregular profile away from a sand pit near Marion, Arkansas (Fig. 1, Table 1). A student field opportunity arose when CERI network personnel were contacted by the owners of an explosives company who were disposing of old chemical explo-

Table 1
Explosion Parameters

Location	Date (mm/dd/yyyy)	Time (UTC)	Latitude (°N)	Longitude (°W)	Size (kg)
Marked Tree, Arkansas	10/29/2002	03:40:00.025	35.46031	90.56528	1134
Mooring, Tennessee	10/30/2002	04:00:00.025	36.33211	89.58719	2268
Marion, Arkansas	04/27/2001	19:02:01.226	35.23014	90.26625	23

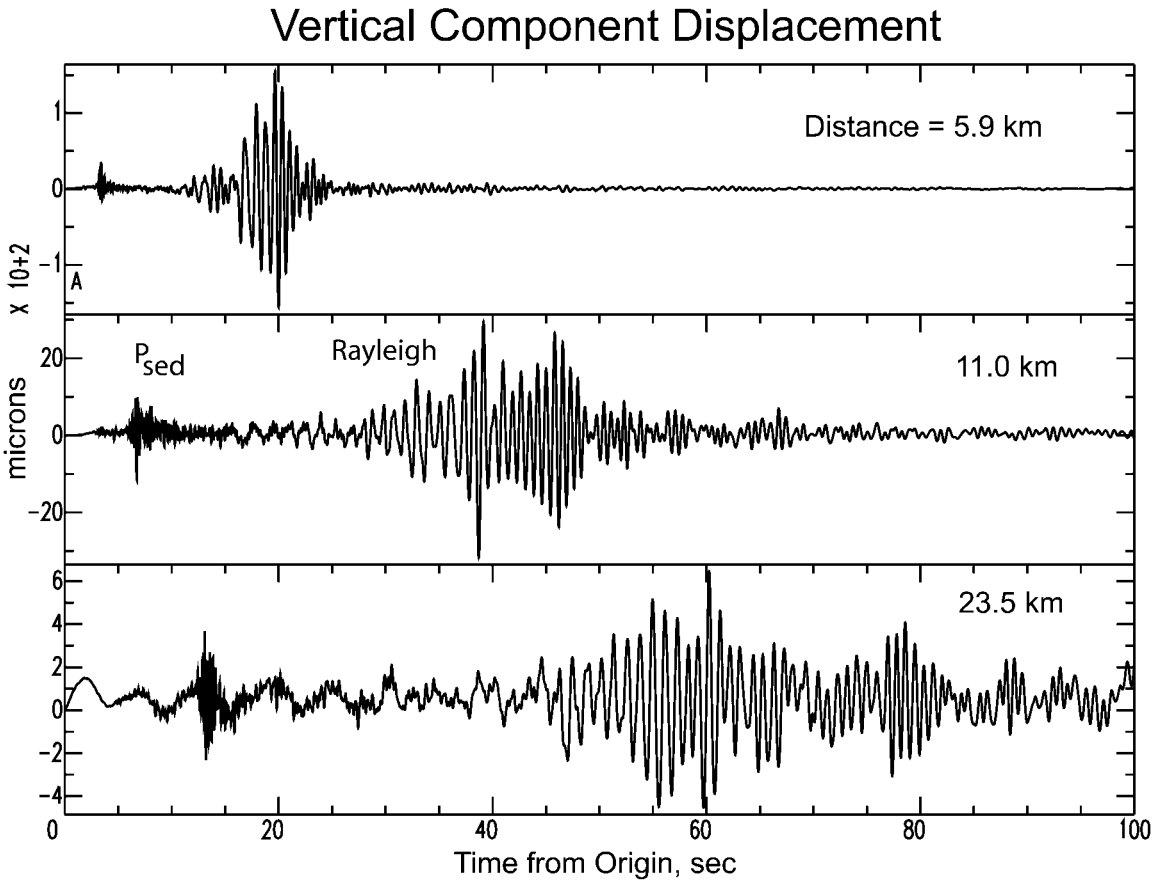

Figure 2. Example of vertical component broadband displacement data showing P_{sed} and Rayleigh waveforms from the Mooring explosion. The character of the seismograms is almost entirely controlled by wave propagation within the thick unconsolidated sediments of the Mississippi embayment.

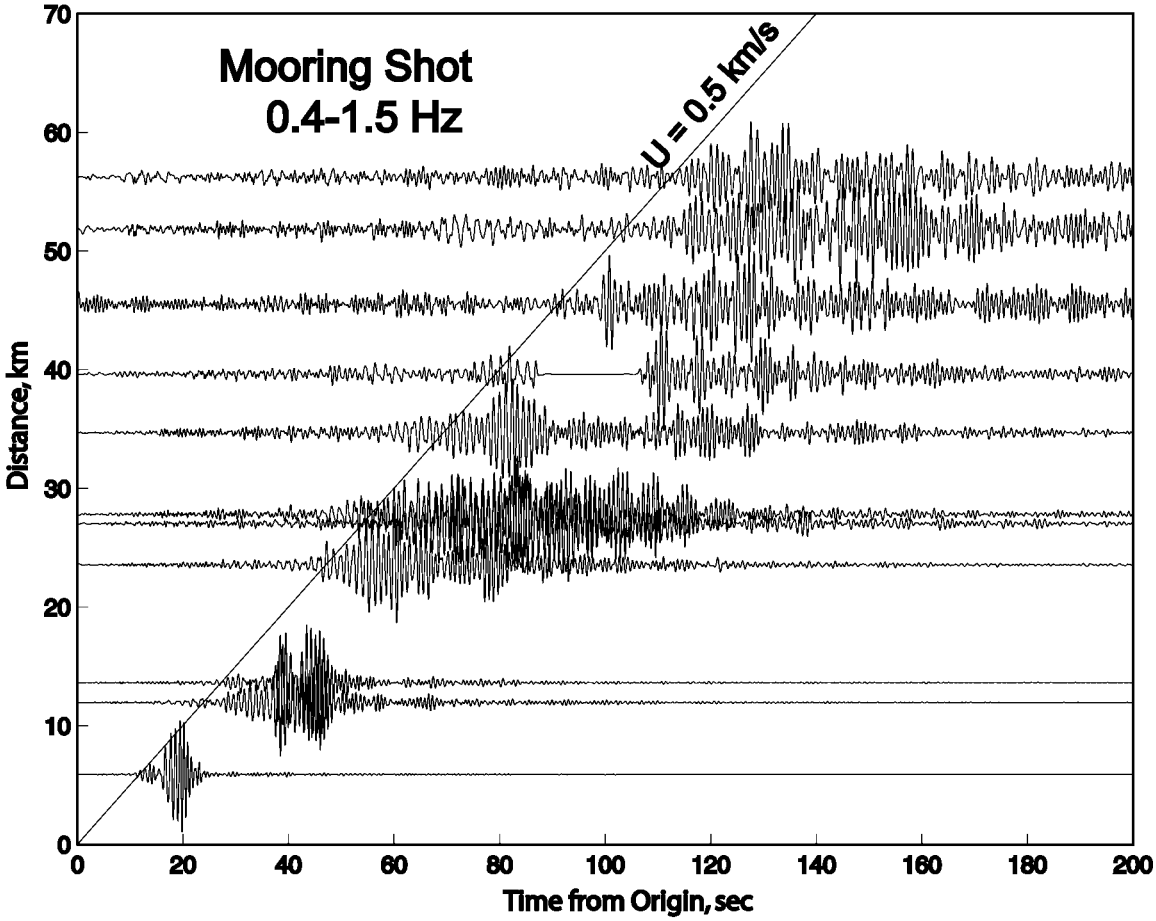

Figure 3. Pseudoprofile of filtered, vertical-component Rayleigh-wave data as a function of distance. The data have been bandpassed filtered between 0.4 and 1.5 Hz to show the prominent short-period sediment Rayleigh waves. A travel-time line for a group velocity of 500 m/sec is plotted on the profile.

sives. An array of 11 three-component K2 accelerographs were deployed in a profile from 14-kg and 23-kg surface explosions. Figure 4 shows ground velocity derived from vertical acceleration observations from the 23-kg explosion. Rayleigh waves of 1–4 Hz propagate to a distance of 3 km from the shot and have group velocities less than 300 m/sec, attesting to the very low shear-wave velocities observed in the upper 100 m of the unconsolidated sediments.

Empirical Q_p and Q_s Analysis

The unconsolidated sediments of the embayment form a very effective seismic wave guide. Figure 5 shows a smoothed version of the velocity model developed by Langston (2003a). Model parameters are tabulated in Table 2. The average properties of this model were constrained using an acoustic well log and travel times of observed earthquake body-wave phases. The V_p/V_s ratio is well constrained by the travel-time data and show very high values of 3 or more. The base of the wave guide consists of high-velocity carbonate rocks. Because seismic-wave velocities generally increase with depth, diving *P* waves from a surface source will refract upwards in the structure and surface waves will be normally dispersed. It can be easily shown using group velocity dispersion curves that surface waves in the frequency band of 0.3 to 4 Hz will consist of many interfering higher modes in addition to the fundamental mode. Indeed, a look at the data in Figure 2 or Figure 3 shows that surface waves consist of several different group arrivals with distance indicative of the interference of higher and fundamental mode surface waves.

Broadband stations that recorded the explosions are broadly distributed within the embayment (Fig. 1). Sediment thickness changes from approximately 500 m to 1000 m over this station distribution. Stations are not confined to a single, simple linear profile from the sources. Thus, the body waves and surface waves generally sample different velocity structure in detail, depending on the location of the source and seismic stations.

Ideally, the analysis of the waveforms must take into account complexity of multimode surface-wave propagation and recognize that structure is heterogeneous and changing

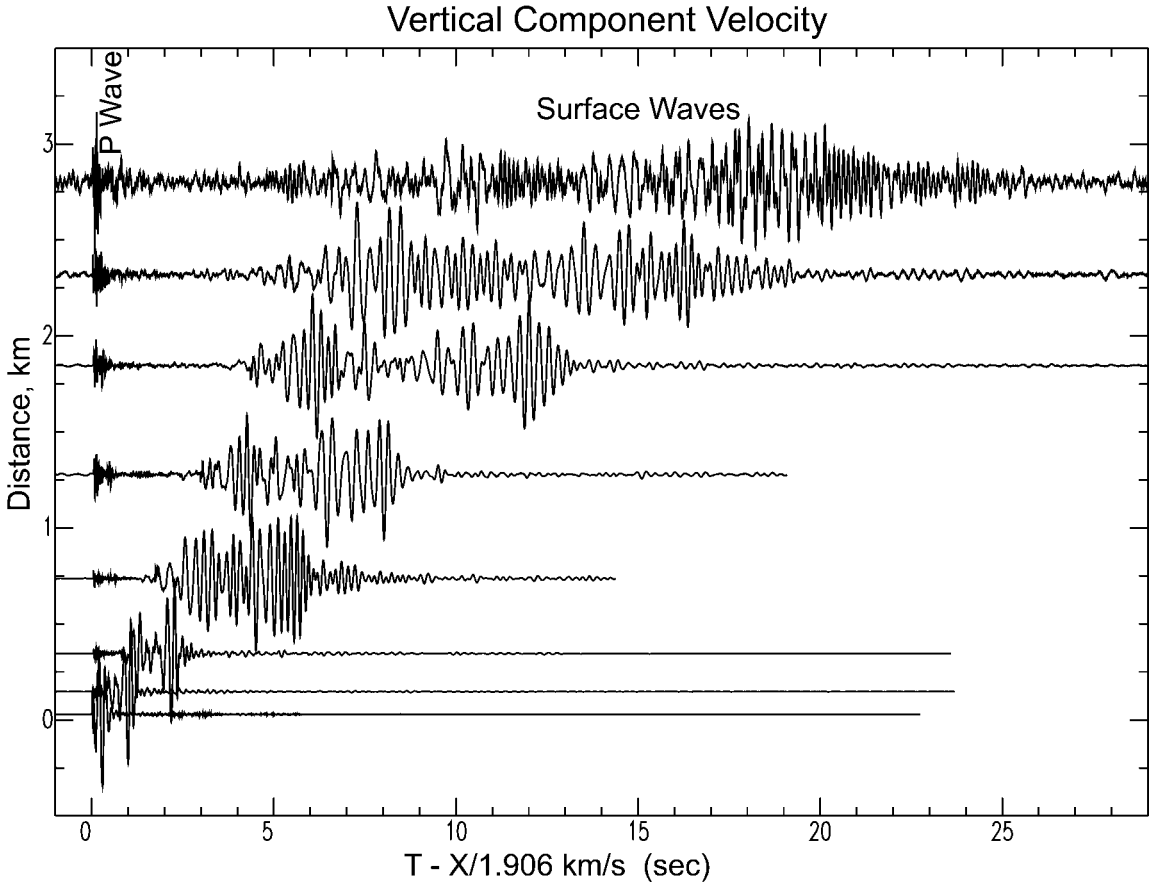

Figure 4. Pseudoprofile of derived vertical-component velocity from accelerograph recordings of the 23-kg Marion explosion showing the sediment *P* wave and long wave trains of the dispersed high-frequency Rayleigh waves. These Rayleigh waves were used to explore distance-attenuation at higher frequencies.

depending on the source to receiver path. However, the effect of attenuation is so large that these issues of heterogeneity and wave propagation amount to second-order effects in the estimate. The approach used here is to cautiously adopt several simplifying assumptions in order to estimate anelastic attenuation, and then to validate these assumptions using synthetic seismograms for an explosion source in plane-layered structure.

The first simplifying assumption is that the observed surface waves can be treated as fundamental mode surface waves in plane layered media. The vertical displacement amplitude spectrum for a fundamental mode Rayleigh wave is given by

$$|\hat{w}(\omega)| = \frac{|\hat{A}(\omega)|e^{-\gamma r}}{r^{1/2}}, \tag{1}$$

where we are using the temporal Q formulation (Aki and Richards, 1980, pp. 296–298) that incorporates group velocity, U, into the distance-attenuation coefficient, γ, by

$$\gamma = \frac{\omega}{2UQ} = \frac{\pi f}{UQ}. \tag{2}$$

Temporal Q is used because group velocity may be measured from wave group arrivals at individual stations. The network is too sparse to measure phase velocity.

The data are analyzed by forming a pseudoprofile with distance, bandpass filtering around a central frequency, computing the envelope of the signal using the modulus of the analytic signal (Farnbach, 1975), and then manually picking the arrival time and amplitude of the peak of the envelope function. Choice of central frequencies for each bandpass filter are shown in later figures, are tabulated in Table 3, and were primarily defined by the available signal-to-noise ratio in the data. The bandpass filter consisted of zero-phase, two-pole butterworth filters with corner frequencies defined around $\pm 5\%$ of the central frequency. Group velocity was determined by computing the slope of the linear time-distance regression fit of the data. The distance attenuation coefficient was computed by first correcting the amplitude data for $r^{-1/2}$ geometrical spreading and then computing the

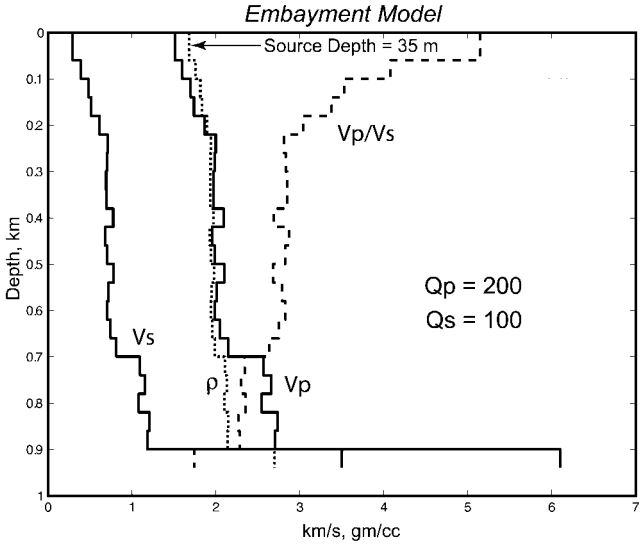

Figure 5. A layered velocity model derived from Langston (2003a) used to construct synthetic seismograms in this paper. Note the large variation in *V*p/*V*s ratio with depth reflecting large changes in porosity within the sediment column. Model parameters are tabulated in Table 2.

Table 2
Sediment Velocity Model

V_p (km/sec)	V_s (km/sec)	Density (gm/cc)	Layer Thickness (km)
1.51000	0.29330	1.67870	0.06
1.60000	0.39220	1.75580	0.04
1.69858	0.48148	1.81542	0.04
1.73872	0.51490	1.83594	0.04
1.86626	0.61454	1.89254	0.04
1.99781	0.71072	1.94192	0.04
1.98329	0.70034	1.93680	0.04
1.97002	0.69080	1.93206	0.04
1.97232	0.69245	1.93288	0.04
2.09177	0.77691	1.97350	0.04
1.95497	0.67993	1.92660	0.04
1.98876	0.70426	1.93874	0.04
2.10138	0.78359	1.97660	0.04
2.01234	0.72107	1.94698	0.04
1.98906	0.70447	1.93885	0.04
2.04542	0.74447	1.95825	0.04
2.14475	0.81358	1.99028	0.04
2.56665	1.09626	2.10592	0.04
2.65975	1.15745	2.12840	0.04
2.54404	1.08136	2.10033	0.04
2.73649	1.20775	2.14631	0.04
2.70346	1.18611	2.13867	0.04
6.10000	3.50000	2.70000	—

slope of the linear fit of the natural log-amplitude-distance data. The statistics of the fit were determined using standard regression formulas.

Figure 6 shows an example result for the 1-Hz bandpass of broadband Rayleigh-wave data. The scatter of travel-time and log-amplitude data about the straight line fit gives an indication of the nature of velocity heterogeneity in the embayment. The waveform data for stations at distances greater than 20 km showed multiple interfering arrivals that were probably due to interfering higher modes or wave multipathing due to velocity heterogeneity. Even so, the Rayleigh waves were observed to travel at such low group velocities that picking other adjacent amplitude peaks had little effect on group velocity or distance decay estimates. Use of all of the time and amplitude data to determine these parameters seems to be a reasonable approach since the standard errors in the fit were generally less than 10% (Table 3) and there were no significant deviations from a linear relationship.

The apparent attenuation at each frequency, Q^{-1}, was derived from equation (2) having the estimates of U and γ. The standard error in the apparent attenuation can be found from a perturbation analysis of equation (2) using the standard errors from the linear fit for U and γ (σ_U and σ_γ, respectively). The result is

$$\sigma_{Q^{-1}} = \frac{[\sigma_\gamma U + \sigma_U \gamma + \sigma_\gamma \sigma_U]}{\pi f}. \quad (3)$$

This was used to determine the error in attenuation displayed in Table 3 and the error bars in subsequent plots.

Figure 7 shows the result for the Rayleigh-wave distance attenuation coefficient, γ, plotted against center frequency. Each coefficient has relatively small error, and the trend of coefficients versus frequency is nearly linear, implying that Q^{-1} is roughly constant with frequency. Because sediment wave velocities are so low the group velocity is also well determined (Fig. 8, Table 3). Combining the group velocity and distance attenuation coefficient to compute apparent Q yields the results shown in Figure 9. Assuming that the apparent Q is most closely related to Q_s is reasonable based on past Rayleigh wave studies but should be treated as a working hypothesis at this point. Figure 9 also includes results from analyzing the data from the 23-kg surface explosion recorded near Marion, Arkansas (Fig. 4). Intermediate results for the small explosion are not shown but are tabulated in Table 3.

The same empirical processing scheme was applied to 3-to 10-Hz P_{sed} waves observed in the ESEE vertical component data except for a different assumed geometrical spreading relationship. P_{sed} is generally composed of postcritical multiple reflections in the unconsolidated sediment wave guide. Ray theory computations for the model of Figure 5 show that the small positive velocity gradient in the model causes progressive, postcritical *P*-wave reverberations to cut out about every 4.5 km in distance from the source. Under this interpretation, the beginning of the P_{sed} wave is a different *P* wave reverberation for differing distances. From 0 to 4.5 km it is composed of the primary reflection, from 4.5 to 9 km the first reverberation of the primary reflection within the sediment column, from 9 to

Table 3
Apparent Attenuation Values

Wave	f (Hz)	U (km/sec)	σ_U km/sec)	γ /km	σ_γ /km	Q^{-1}	$\sigma_Q{}^{-1}$	Q	Q_{min}	Q_{max}
R	0.4	0.791	0.029	7.62×10^{-3}	5.60×10^{-3}	4.80×10^{-3}	3.83×10^{-3}	208	116	1034
R	0.5	0.680	0.021	1.03×10^{-2}	6.63×10^{-3}	4.47×10^{-3}	3.09×10^{-3}	224	132	726
R	0.6	0.613	0.069	3.52×10^{-2}	5.42×10^{-3}	1.14×10^{-2}	3.25×10^{-3}	87	68	122
R	0.7	0.511	0.043	3.56×10^{-2}	4.92×10^{-3}	8.29×10^{-3}	1.95×10^{-3}	121	98	158
R	0.8	0.531	0.029	4.55×10^{-2}	4.53×10^{-3}	9.62×10^{-3}	1.55×10^{-3}	104	89	124
R	0.9	0.392	0.017	5.32×10^{-2}	3.05×10^{-3}	7.37×10^{-3}	7.60×10^{-4}	136	123	151
R	1.0	0.387	0.023	6.79×10^{-2}	5.83×10^{-3}	8.36×10^{-3}	1.26×10^{-3}	121	104	141
R	1.1	0.371	0.028	9.41×10^{-2}	5.28×10^{-3}	1.01×10^{-2}	1.39×10^{-3}	99	87	115
R	1.2	0.373	0.030	1.05×10^{-1}	6.90×10^{-3}	1.04×10^{-2}	1.58×10^{-3}	96	83	113
R	1.3	0.363	0.039	1.12×10^{-1}	1.38×10^{-2}	1.00×10^{-2}	2.42×10^{-3}	100	81	132
R	1.5	0.315	0.015	6.39×10^{-2}	1.70×10^{-1}	4.27×10^{-3}	1.21×10^{-2}	234	61	inf
R	2	0.273	0.023	2.15×10^{-1}	1.37×10^{-1}	9.35×10^{-3}	7.26×10^{-3}	107	60	480
R	3	0.129	0.003	6.79×10^{-1}	2.68×10^{-1}	9.30×10^{-3}	3.99×10^{-3}	108	75	189
R	4	0.122	0.008	1.32	2.05×10^{-1}	1.29×10^{-2}	3.03×10^{-3}	77	62	101
P	3	1.71	0.086	3.38×10^{-2}	9.15×10^{-3}	6.14×10^{-3}	2.05×10^{-3}	163	122	245
P	4	1.97	0.101	3.45×10^{-2}	9.62×10^{-3}	5.41×10^{-3}	1.87×10^{-3}	185	137	282
P	5	1.77	0.014	4.01×10^{-2}	8.22×10^{-3}	4.52×10^{-3}	9.70×10^{-4}	221	182	282
P	6	1.87	0.047	4.41×10^{-2}	6.59×10^{-3}	4.39×10^{-3}	7.84×10^{-4}	228	193	277
P	7	1.74	0.042	6.04×10^{-2}	1.24×10^{-2}	4.78×10^{-3}	1.12×10^{-3}	209	169	273
P	8	1.97	0.075	5.94×10^{-2}	1.36×10^{-2}	4.66×10^{-3}	1.28×10^{-3}	214	168	296
P	9	1.91	0.092	6.06×10^{-2}	1.71×10^{-2}	4.08×10^{-3}	1.41×10^{-3}	245	182	374
P	10	1.63	0.083	6.53×10^{-2}	4.43×10^{-2}	3.38×10^{-3}	2.58×10^{-3}	296	168	1255

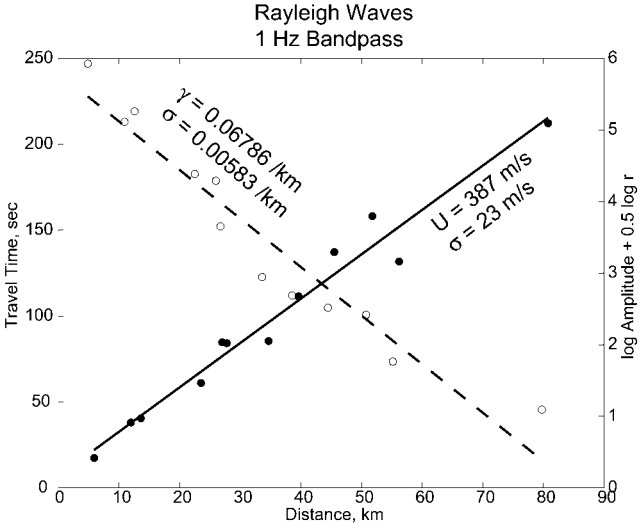

Figure 6. Example of regression fits of arrival time–distance and log amplitude–distance data for 1-Hz Rayleigh waves that were used to derive the distance attenuation coefficient, γ, and the group velocity, U. Also shown are the inferred standard errors.

13.5 km the second reverberation, and so on. P_{sed} begins with the sixteenth reverberation of the primary reflection at 80 km distance in the vertically inhomogeneous model. This behavior is similar to the propagation of the *Lg* phase which is composed of progressive postcritical *S*-wave reverberations in the crustal wave guide (Vogfjord and Langston, 1996; Langston *et al.*, 2002b). Since, P_{sed} is primarily a trapped, largely horizontally propagating set of body waves in the sedimentary wave guide there is an ambiguity for the choice of geometrical spreading in the simple wave propagation model used to explain its behavior with distance. On one hand, if the wave guide is efficient enough, all *P*-wave energy may be trapped within it so that the entire wave packet should have a 2D geometrical spreading like a Rayleigh wave, or $r^{-1/2}$. On the other hand, the practical data analysis activity of choosing the peak amplitude of P_{sed} will likely sample a particular, single ray multiple that should have a well-defined 3D geometrical spreading of r^{-1}. We will investigate both geometrical spreading assumptions in the analysis.

Figure 10 shows estimated Q_p for the P_{sed} wave as a function of center frequency assuming r^{-1} geometrical spreading. Relative errors are large because the attenuation coefficient is smaller than Rayleigh-wave values with larger relative variance and higher group velocity (equation 3). Values range from about 160 at 3 Hz to about 300 at 10 Hz.

Synthetic Seismogram Analysis

The empirical analysis has many assumptions that must be checked. Although the peak amplitude of the Rayleigh or P_{sed} envelope was taken at each test frequency, the data clearly showed multiple arrivals around those peaks that probably indicate additional modes or multipathed waves. The assumption of fundamental mode wave propagation needs to be checked for the Rayleigh data interpretation and geometrical spreading must be checked for the P_{sed} wave. There is even a question of the correct physical interpretation of the apparent Q since it depends on definitions of temporal

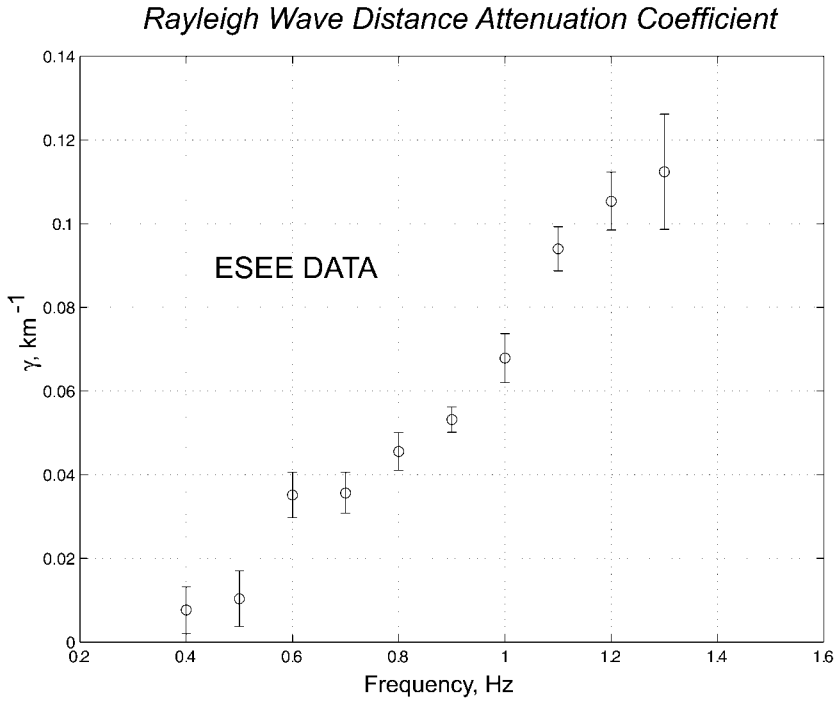

Figure 7. Summary of the Rayleigh-wave distance attenuation coefficient versus frequency.

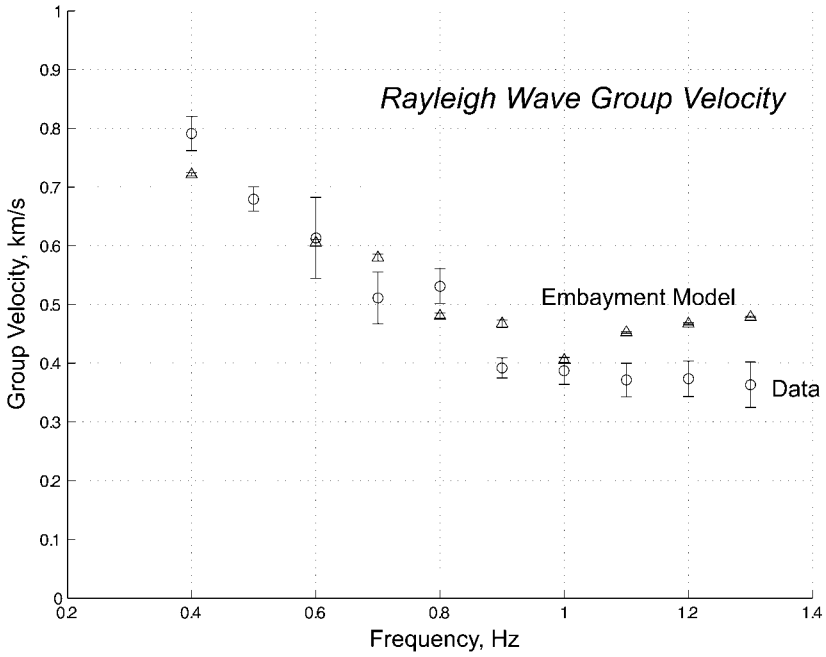

Figure 8. Summary of observed (circles) and synthetic (triangles) apparent Rayleigh-wave group velocity as a function of frequency.

and spatial attenuation for dispersed waves. Q_p and Q_s are usually defined as specific elastic layer parameters in wave propagation codes and have clear physical meaning as the anelastic material property. The apparent Q values determined from the data are, at best, smoothed averages of some Q_p and Q_s profile with depth (Ben-Menahem and Singh, 1978).

We use a modified Filon method for wavenumber integration of the response of a moment-tensor point source in plane-layered media (Apsel, 1979; Barker, 1984). The displacement response for an isotropic point source at 35-m depth in the model displayed in Figure 5 was computed for ranges between 10 and 100 km. Causal anelasticity is included in the computation through use of the Futterman (1962) attenuation operator where complex velocity, V_{eff}, is introduced through

$$\frac{1}{v_{\text{eff}}} = \frac{1}{v}\left\{1 - \frac{1}{\pi Q}\ln\left(\frac{\gamma_0\omega}{\omega_0}\right) - \frac{i}{2Q}\right\} \qquad (4)$$

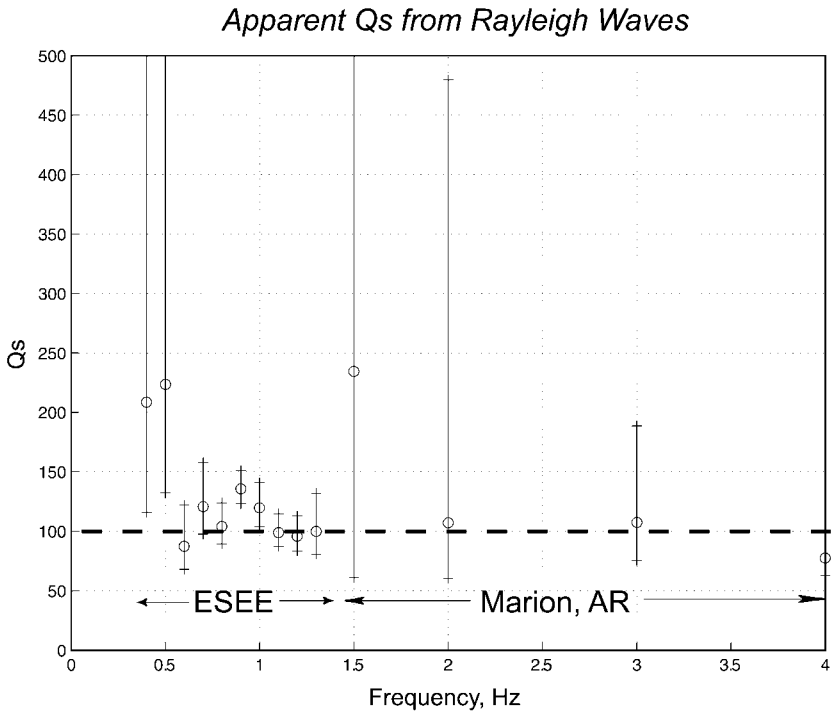

Figure 9. Summary of apparent Q_s for the Rayleigh-wave data from ESEE and the Marion explosion as a function of frequency. The minimum and maximum values were computed from the standard errors inferred from Q^{-1} shown in Table 3.

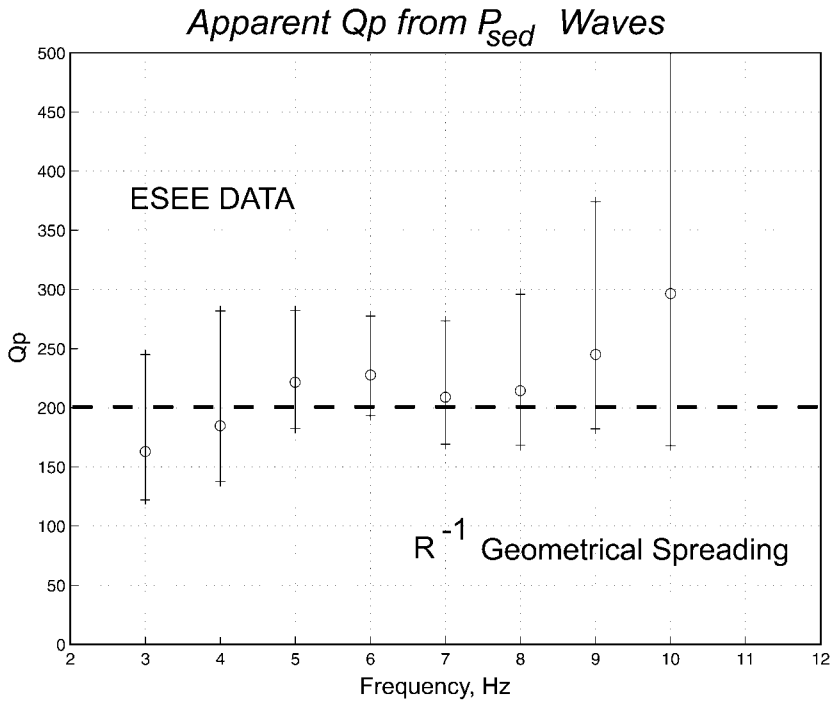

Figure 10. Summary of apparent Q_p for the P_{sed} data from ESEE. Same scheme as Figure 9.

and where v is the elastic velocity (V_p or V_s), Q is either Q_p or Q_s, γ_0 is Euler's constant, and ω_0 is a low-frequency cutoff frequency for the attenuation band.

A variety of Q models were assumed in the synthetic seismogram computations. The simplest model was for constant Q_p and Q_s where we parsimoniously assume constant values of 200 and 100, respectively. These values seem reasonable considering the error bars in the data shown in Figures 9 and 10. Subjecting the synthetic seismograms (Fig. 11) to the same analysis for apparent distance attenuation and group velocity yields the group velocity results shown in Figure 8, Q_s results from Rayleigh waves in Figure 12, and Q_p results from P_{sed} waves in Figure 13.

First we note that the synthetic seismograms generally yielded unambiguous estimates of group velocity from the maximum amplitude peaks of Rayleigh waves as a function

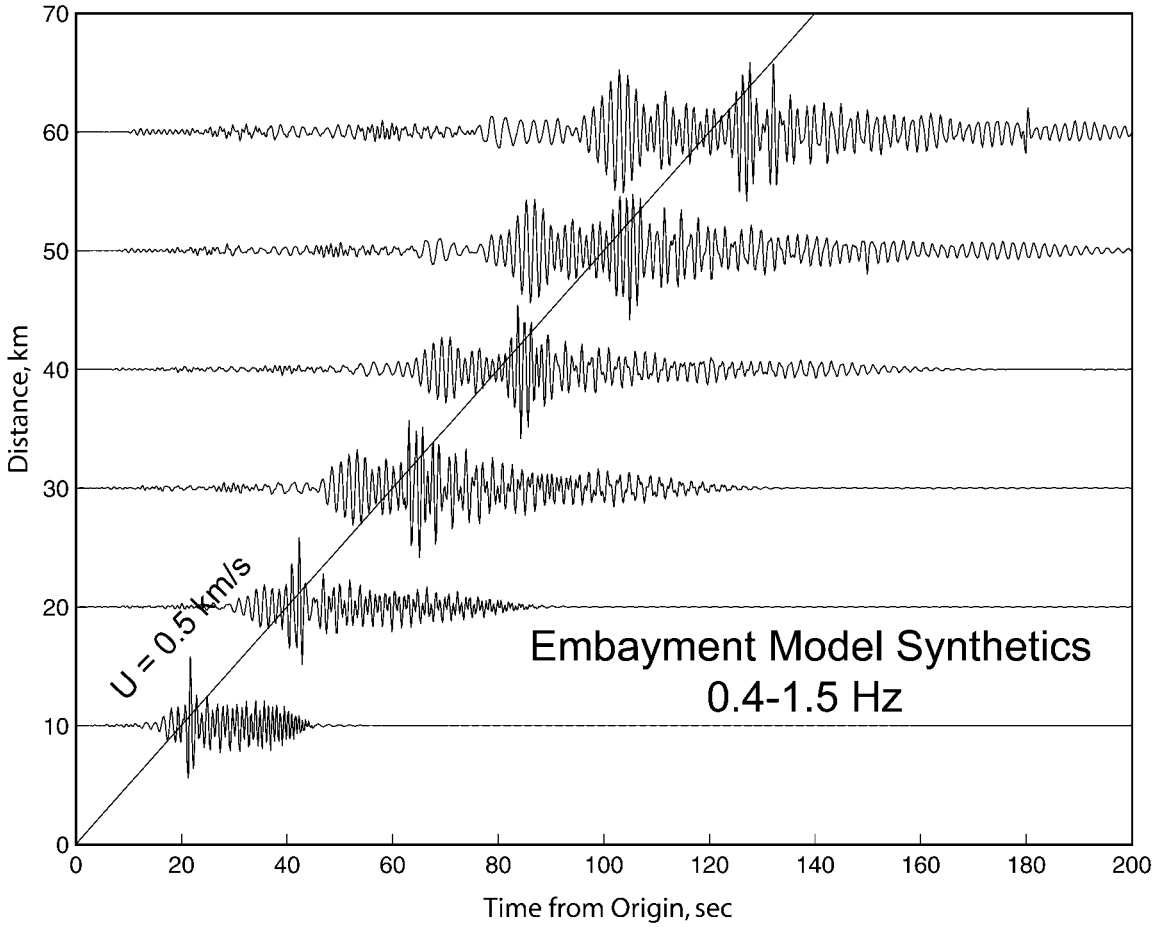

Figure 11. Bandpass-filtered synthetic seismograms computed for the sediment model shown in Figure 5. Same scheme as Figure 3.

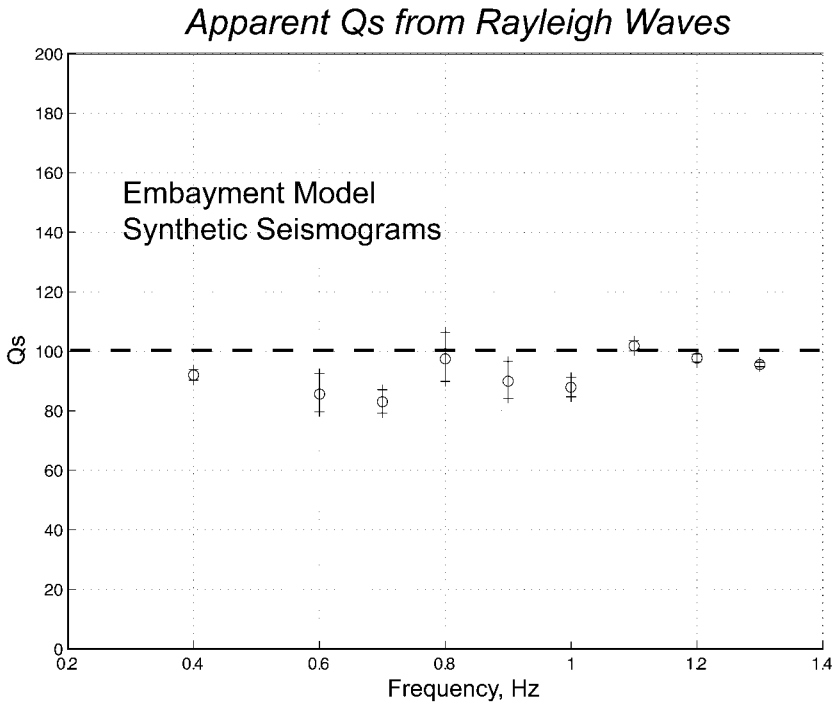

Figure 12. Apparent Q_s inferred from the synthetic Rayleigh waves. The dotted line shows the input model value. Q_s is generally underestimated because of the interference of higher mode Rayleigh waves at closer distances.

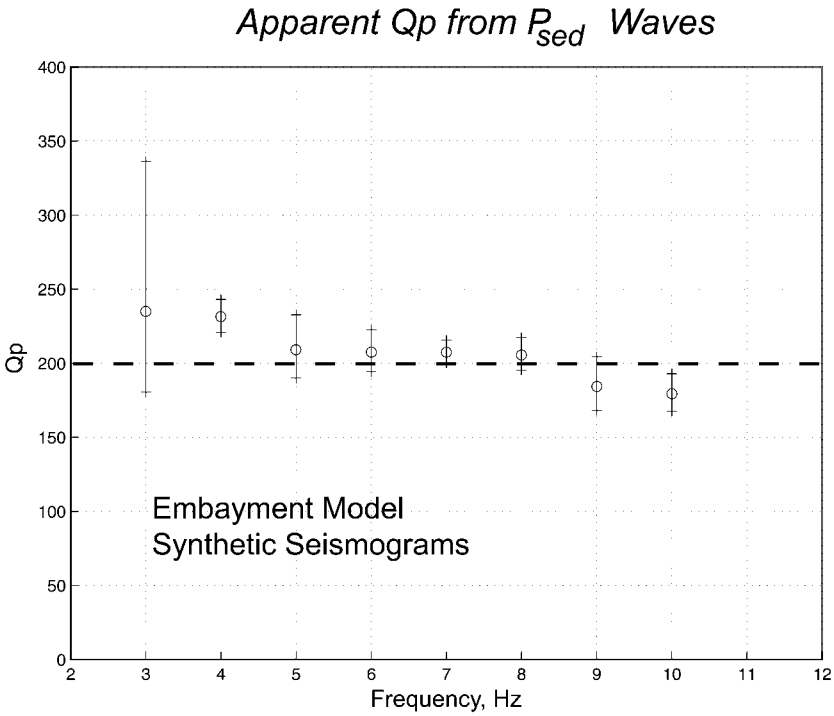

Figure 13. Apparent Q_p inferred from the synthetic P_{sed} waves. The dotted line shows the input model value. The Q_p determinations have surprisingly high variances because of higher group velocities and interference of several multiple sediment reflections at each range.

of frequency (Fig. 8). However, for center frequencies less than 1 Hz, these peaks clearly consisted of various higher modes that interfered with each other as a function of distance from the source. In fact, interference of modes made it impossible to find an estimate of group velocity at 0.5 Hz. For frequencies higher than 1 Hz, the synthetic data were composed of fundamental mode surface waves but yielded group velocities about 100 m/sec higher than the observed group velocities. Comparison of apparent group velocities for the synthetics and the ESEE data shows that model wave velocities are slightly too fast in the upper third of the model. This is consistent with the results of Langston (2003a, 2004) showing that there is a universal near-surface, very low velocity layer within the sediments of the Mississippi embayment. This layer is not included in the model displayed in Figure 5.

The interference of the higher modes in the synthetic seismogram computations actually produces considerable scatter in the amplitude determinations and causes Q_s to be underestimated by as much as 20% for frequencies less than 1 Hz. This is because the analysis method is based on picking peak motions that may be composed of one or more surface-wave arrivals. Interference is greatest at closer ranges where the arrival times of several higher modes are most similar. Dispersion allows the various modes to separate at greater ranges. Thus, the combination of arrivals at close range results in higher amplitude, and dispersion produces lower amplitude at greater ranges, producing a greater distance decay rate and, hence, lower apparent Q estimate. It is worth noting that when the Rayleigh waves are truly fundamental mode, as for frequencies greater than 1 Hz, the Q estimates are within a few percent of the input Q_s verifying that the assumption of temporal Q in the analysis is consistent with the spatial Q_s in the synthetic seismogram computation.

A similar interference effect occurs for Q_p estimates using the P_{sed} phase (Fig. 13). P_{sed} at each range consists of several higher-order P-wave reverberations within the ideal structure. Regressing these amplitudes and arrival times over the entire distance range to find an average group velocity and amplitude decay mixes the behavior of, perhaps, a dozen separate body-wave arrivals. The resulting Q_p values have surprisingly large errors from the regression analysis but are close to the input Q_p value of 200 (Fig. 13) when a geometrical spreading of r^{-1} is assumed. Assuming $r^{-1/2}$ geometrical spreading produces apparent Q_p values 25% lower than input in the synthetic model.

Discussion

If we assume that the synthetic seismograms computed for an ideal, plane-layered embayment model reflect the same kind of wave propagation effects that exist in the data, then it appears that Q_s estimates from the Rayleigh-wave data may be underestimated by up to 20%. However, there is an important additional wave propagation effect that clearly exists in the observed data that is not included in the theoretical calculations. This is the effect of scattering from velocity heterogeneity.

General characteristics of the data include multiple group arrivals around the maximum amplitude arrival at any frequency, long-duration Rayleigh wave codas, and significant off-azimuth scattered energy as seen in the transverse component. Figure 14 shows an example of three-

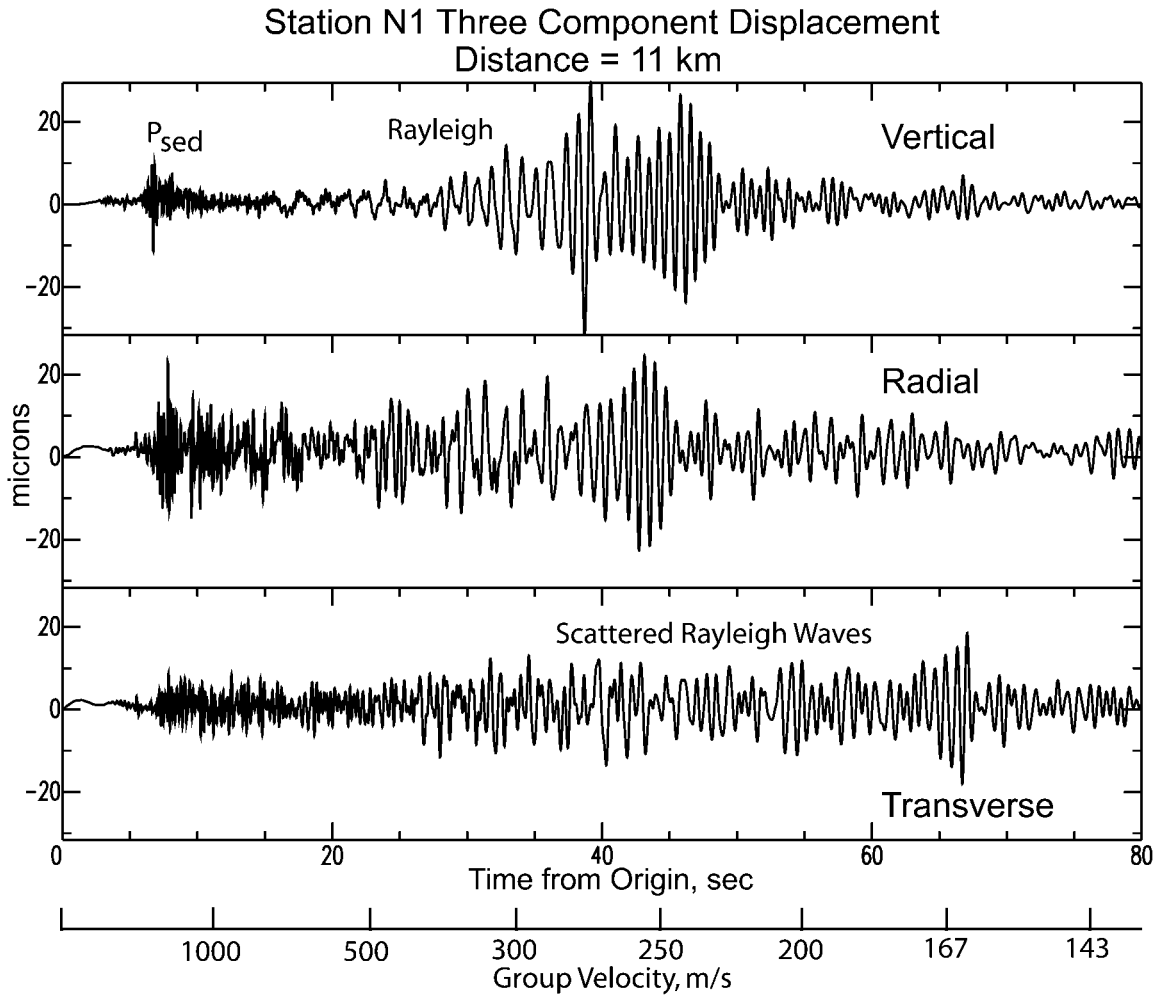

Figure 14. Vertical, radial (away from the source), and transverse displacements for a broadband station 11 km from the Mooring explosion. The data are plotted versus time and group velocity. Note the relatively large transverse component of motion showing presumed scattered Rayleigh waves, a scattered P_{sed} wave, and relatively large coda after the Rayleigh-wave arrival. The transverse component theoretically should show no motion for an axisymmetric isotropic source. The data imply significant velocity heterogeneity that is a significant contribution to the apparent attenuation.

component waveforms for a station 11 km from the source. The transverse horizontal component (orthogonal to the radial component) shows significant ground motions at nearly the same amplitude as the vertical or radial Rayleigh-wave arrival. The coda of the transverse component is lengthy and contains major arrivals with very low apparent group velocities. The transverse component even shows a high-amplitude high-frequency P_{sed} phase with associated high-frequency coda. These characteristics are strongly suggestive of wave scattering in heterogeneous velocity structure and are not particularly surprising considering the heterogeneous geological structure of an active river flood plain.

The separation of effects of anelastic attenuation from those involving wave scattering is a well-known seismological problem (e.g., Frankel and Wennerberg, 1987). Inclusion of anelastic and scattering attenuation into wave propagation theories often involve the same functional dependence and results in a complete tradeoff between the effects. Commonly (Dainty, 1981), the total attenuation, Q^{-1}, is just

$$Q^{-1} = Q_{\text{Instrinsic}}^{-1} + Q_{\text{Scattering}}^{-1} . \quad (5)$$

In this study we have assumed that there has been no contribution from scattering attenuation. Our estimates of intrinsic attenuation, therefore, must be maximum values or, conversely, the estimates of Q_s and Q_p must be minimum bounds on the intrinsic Q of the unconsolidated embayment sediments.

Several past studies of bulk sediment anelasticity in the embayment derived from earthquake *P*-and *S*-wave spectra and *S/Sp* spectral ratios report values of Q_s ranging from 25

to 40 and Q_p ranging from 25 to 60 (e.g., Liu *et al.*, 1994; Chen *et al.*, 1994), 2.5 to 4 times smaller than the values obtained here. The Rayleigh-wave and P_{sed} data are clearly inconsistent with the previously determined low Q values. The Rayleigh-wave frequency band overlaps the *S/Sp* spectral ratio data at its low end, but the P_{sed} data occurs directly in the center of *S/Sp* spectral ratio band. Several synthetic seismogram calculations for the low values were performed and demonstrated that it would be unlikely that these waves could even be observed past ranges of 20 km. The difference in distance-amplitude decay results in Rayleigh-wave amplitudes being different by several orders of magnitude at the greatest ranges. The empirical analysis is very sensitive to bulk attenuation in the sediments and easily resolves the difference between low- and high-Q models.

For example, Figure 15 shows a comparison of synthetic seismograms computed using our Q values and previous values with the vertical displacement data observed at Glass, Tennessee (GLAT). GLAT is only 28 km from the source. The synthetic seismogram computed using the low Q values is highly attenuated relative to the high-Q synthetic. Most of the Rayleigh-wave train has been removed by absorption, relative to the longest period Rayleigh waves seen at about 40-sec arrival time. Even the P_{sed} phase has been reduced in the low-Q synthetic so that it is scarcely larger than the lowest frequency Raleigh wave (at 40-sec arrival time). The high-Q synthetic, on the other hand, matches the general character of the data in frequency content, amplitude, duration, and arrival time of the major P-and surface-wave arrivals.

The issue remains of how our present results relate to the much higher frequency geotechnical results of Wang *et al.* (1994) and Pujol *et al.* (2002). If Q is related to anelastic material properties and is independent of frequency, then low values of 10 to 34 in the upper 60 m would imply that Q must increase significantly with depth in the unconsolidated sediments. However, trial synthetic seismogram calculations assuming a low Q_s of 30 in the upper 100 m of the

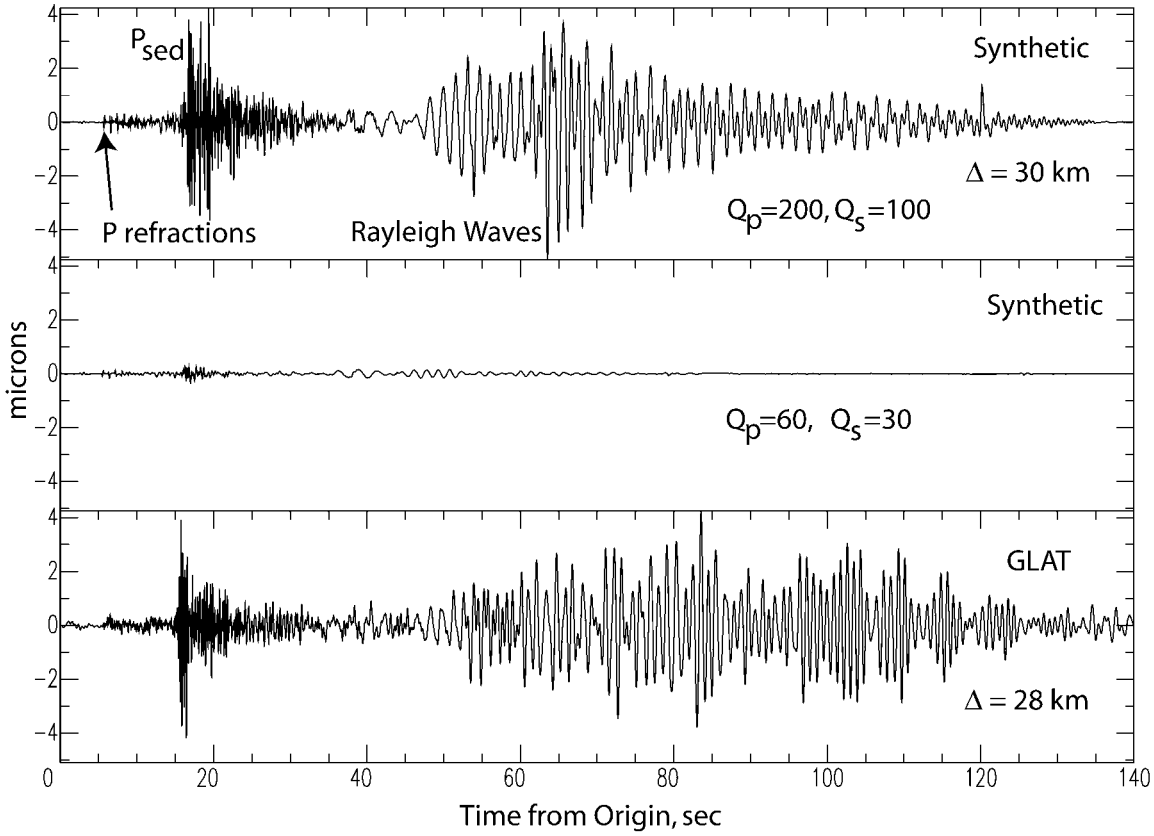

Figure 15. Comparison of synthetic seismograms with the observed vertical displacement data at Glass, Tennessee (GLAT). A 2-pole, causal butterworth bandpass filter with corner frequencies of 0.5 and 8 Hz was applied to the data and synthetics because of the large amount of ambient ground noise below 0.5 Hz contained in the data. The synthetic waveforms were constructed using the velocity model in Figure 5 with the simple Q models as annotated in the figure. An isotropic source with a depth of 35 m was also assumed. This figure shows the large effect that Q_s and Q_p have on the distance-attenuation of both P and Rayleigh waves. The low-Q model synthetic, if examined in detail, does not show appropriate frequency content, relative phase amplitudes, or wave-train durations.

velocity model showed that 1-Hz fundamental mode Rayleigh waves were actually significantly attenuated with the attenuation being inconsistent with the observations. This could imply that Q is frequency dependent, that Q is sensitive to differing wave scattering mechanisms between the three kinds of experiments, or a combination of both. We leave this interesting anomaly to future analysis but recognize that is an outstanding, important issue.

Our results imply that high-frequency earthquake ground motions will not be appreciably attenuated from passage through the sediment column. A 5-Hz shear wave, for example, traveling 1 km in a medium (V_s = 0.6 km/sec) with an average Q_s of 30 will loose 58% of its amplitude. Only 22% of wave amplitude will be lost if the Q_s is 100. Thus, considering small-strain amplitude seismic waves, 5-Hz shear waves should be generally amplified by the embayment sediments since the impedance decrease of the sediments should dominate over the attenuation effect.

A second challenge posed by lower-than-expected attenuation in Mississippi embayment sediments is perhaps more profound for earthquake hazards. As our ESEE results show, high-Q but low-velocity sediments form an efficient wave guide that may be expected to allow seismic waves within it to propagate over long distances. This mode of propagation will promote long surface-wave trains with 1- to 3-sec periods, with large amplitudes. These surface waves would have many cycles of high strains that could cause ground failure and liquefaction to long distances and could damage structures large enough to resonate at these long-periods. This sort of hazard is generally not considered by most seismic hazard studies but could be an important concern in the Mississippi embayment. It would not be as important if sedimentary Q was small, but the values we estimate suggest this should be considered an important contributor to hazard. Shallow earthquakes or the shallow part of large ruptures would best energize the sediment wave guide, and the effect might be completely masked in observations from deeper small earthquakes. To illustrate, we show seismograms from an M 4.5 earthquake in Bardwell, Kentucky, on the 6 June 2003 (Fig. 16) recorded at a broadband seismic station 136 km away. The earthquake was 2 km deep, but still put significant energy into the sedimentary wave guide. As our synthetic seismogram models show with low Q, we should not expect to see such large surface waves essentially trapped within the shallow unconsolidated sediments (with group velocities of 400 m/sec and less), which appear from 300 to 500 seconds later at this distance.

In the early stages of this study there was a hope that the combined use of the Rayleigh-wave and P_{sed} data could place constraints on the depth profile of attenuation. Fundamental mode Rayleigh waves, for example, should progressively sample deeper into the sediment column as wave frequency decreases. We effectively get some of this depth dependence in the data and synthetics because higher Rayleigh modes dominate the signal at lower frequencies. However, the resulting empirical Q_s estimates reflect averages of several regions of the sediment profile rather than just the deeper parts. This was borne out by construction of numerical derivatives of the time series using perturbations of the Q profile with depth and processing the data to obtain the distance attenuation coefficient in the same way as the empirical analysis. Existence of multimode surface waves in the analysis produced relatively large variances in the attenuation estimates. The variances of the synthetic estimates were too large to justify modeling the small frequency-dependent variations seen in the empirical determinations (e.g., Fig. 9).

Results from the P_{sed} phase suggest a robust bulk attenuation determination since P_{sed} consists of whole-layer multiples that sample the entire sediment layer many times depending on propagation distance. The inferred value of Q_p (Fig. 10) actually increases at the highest frequencies, but the variance of the estimate also increases. At this point in time, the simplest interpretation for Q structure in embayment sediments is that Q_s and Q_p are constant with depth and with frequency. Frequency-dependent Q models are not required by the data at the level of resolution found from the regression fits of time and amplitude data.

Clouser and Langston (1991) discuss the physical interpretation of sediment Q models. In particular, Q_p and Q_s can be related through wave scattering mechanisms and anelasticity of poroelastic media. A common theoretical relationship is often examined to infer the mechanism of anelastic loss in the material by splitting loss in shear (Q_S^{-1}) from loss in volumetric strain or bulk loss (Q_k^{-1}) (Vassiliou *et al.*, 1982):

$$Q_p^{-1} = LQ_S^{-1} + (1 - L)Q_k^{-1}, \tag{6}$$

where

$$L = \frac{4}{3}\left[\frac{V_s}{V_p}\right]^2. \tag{7}$$

The average V_p/V_s ratio for embayment sediments is well known and is very close to 3 so L = 0.1481 (Langston, 2003a). If there is only loss in shear (Q_k^{-1} = 0), then the inferred Q_p of 200 implies a Q_s of only 30, inconsistent with the inferred value. Assuming Q_s = 100 and Q_p = 200 yields Q_k = 242 for embayment sediments. Thus, significant attenuation occurs in compression as well as shear, not considering loss due to scattering.

It is noteworthy that the present attenuation estimates are most consistent with those of Kang and McMechan (1994) who used controlled source refraction data and examined the scattering characteristics of high-frequency direct P and S waves within the NMSZ within a distance range of 6 to 10 km. They obtained Q_p = 200 and Q_s = 68. However, it is clear from the data that they used that the attenuation that they measured is actually appropriate for the

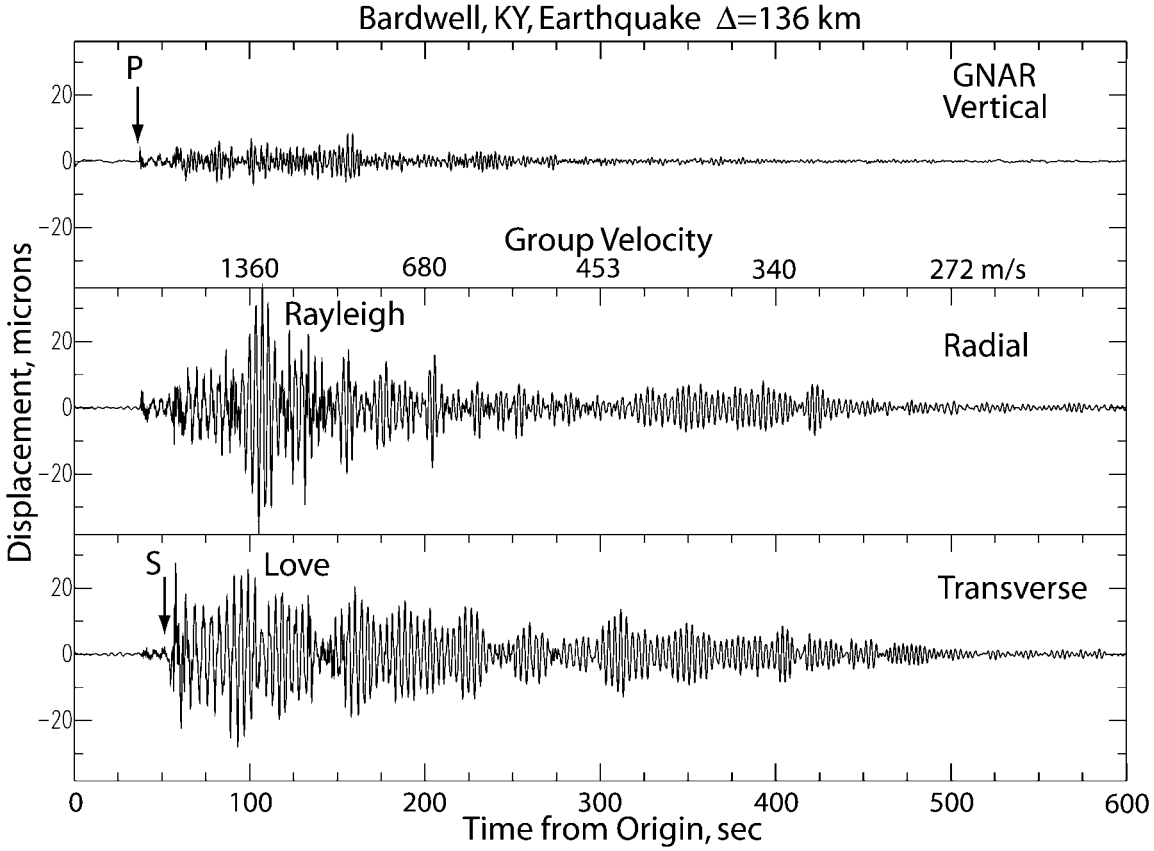

Figure 16. Vertical, radial, and transverse displacement data recorded at Gosnell, Arkansas (GNAR), for a recent moderate earthquake (M 4.5) that occurred at Bardwell, Kentucky. Even at this distance of 136 km, the data show high-amplitude, long-duration surface waves. Rayleigh and Love waves with group velocities of less than 400 m/sec have been excited by this shallow earthquake ($h = 2$ km) and propagate almost entirely within the unconsolidated sediments. The unconsolidated sediments of the Mississippi embayment form an efficient wave guide for waves radiated by shallow events and large events that may rupture into the sediments.

portion of the refracted wave paths that exist within the basement rocks and not the unconsolidated sediments. Therefore, this agreement is fortuitous and cannot be used for support of the values found from sediment Rayleigh and *P* waves.

Results of this study provide additional evidence that past body-wave spectral studies to obtain anelastic attenuation have been strongly influenced by wave scattering mechanisms in the embayment sediment velocity structure and from seismograph installation practices (Langston, 2003b). K (Kappa) and f_{max} spectral parameter estimations depend on elastic-wave propagation effects as well as anelastic attenuation. These results underline the need to test seismological hypotheses (models) using independent means to arrive at realistic bounds on wave propagation parameters.

Conclusions

Lower bounds on Q_s and Q_p have been determined for the thick unconsolidated sediments of the Mississippi embayment using explosion-generated Rayleigh waves and *P* waves. Based on the scatter in the arrival-time and amplitude data, we favor a simple Q model that is independent of frequency and depth. Values of 100 for Q_s and 200 for Q_p explain the distance decay of fundamental and higher mode Rayleigh waves and high-frequency P_{sed} waves. These values are robust and are 2.5 to 4 times larger than previously estimated values from earthquake body-wave spectra. Because scattering is an obvious attribute of the observed waveform data, these anelastic Q estimates must be minimum values; Q_s and Q_p are very likely higher for these thick, unconsolidated sediments. Higher Q implies that 5-Hz shear waves should be amplified by the embayment sediments since the impedance decrease of the sediments should dominate over the attenuation effect. These higher Q values also imply that the thick sediments of the Mississippi embayment will form an efficient wave guide for the propagation of high-amplitude surface waves from shallow earthquakes in the NMSZ.

Acknowledgments

The experimental portion of this work could not have been completed without the help of many people. We appreciate the assistance of Ed Criley and Tom Burdett of the USGS who helped design the ESEE borehole shot points. Jack Van Schaack and Ron Kaderabek graciously came out of retirement to load and detonate the ESEE explosions. CERI technical personnel Greg Steiner, Jim Bollwerk, Chris McGoldrick, and John Filipcic ably managed logistics and helped install field stations during ESEE. Buddy Schweig and Joan Gomberg of the USGS office at CERI arranged for illuminating education and outreach events during the experiment. We appreciate graduate students Ivan Rabak, Daejin Kang, and Qingwen Miao for their help with instrumentation preparation and installation. Jim Dorman graciously volunteered to find sites for temporary stations in the central NMSZ. Appreciation is given to Charles Glover of the Ritter Land and Seed Co. for their help in siting the Mark Tree, Arkansas, source and to James Eddlemon of Mooring, Tennessee, for help in siting the Mooring source. We thank the owners of Omni Explosives Company for using their property to install a seismograph and for allowing us to record their test explosions. In addition, we thank Jim Fowler and Noel Barstow of IRIS/PASSCAL for their help in providing eight broadband instruments for the temporary deployment. Alemayehu Jemberie provided some useful comments on an early version of the manuscript. David Boore, Francis Wu, and Chandon Saikia provided useful review comments. This research was supported by the U.S. Department of the Interior, U.S. Geological Survey under Grant. 02HQGR007 and by the National Science Foundation Mid America Earthquake Center under Project HD-5. We also thank the University of Memphis for providing seed support through a Faculty Research Grant. Use of the Generic Mapping Tool, program for Figure 1 (Wessel and Smith, 1998) is gratefully acknowledged. The Seismic Analysis Code (Goldstein *et al.*, 2002) was used for much of the analysis.

References

Aki, K. (1988). Local site effects on strong ground motion, in *Earthquake Engineering and Soil Dynamics II—Recent Advances in Ground-Motion Evaluation*, J. L. V. Thun (Editor), American Society of Civil Engineers, Park City, Utah, 103–155.

Aki, K., and P. G. Richards (1980). *Quantitative Seismology—Theory and Methods*, W. H. Freeman and Co., San Francisco, California, p. 298.

Apsel, R. (1979). Dynamic Green's functions for layered media and applications to boundary value problems, *Ph.D. Thesis*, University of California, San Diego.

Barker, J. S. (1984). A seismological analysis of the May 1980 Mammoth Lakes, California, earthquakes, *Ph.D. Thesis*, Pennsylvania State University, State College.

Barker, T. G., and J. L. Stevens (1983). Shallow shear wave velocity and Q structures at the El Centro strong motion accelerograph array, *Geophys. Res. Lett.* **10,** no. 9, 853–856.

Ben-Menahem, A., and S. J. Singh (1978). *Seismic Waves and Sources*, Springer-Verlag, New York.

Bodin, P., and S. Horton (1999). Broadband microtremor observation of basin resonance in the Mississippi embayment, central U.S.: implications for seismic hazard assessment, *Geophys. Res. Lett.* **26,** 903–906.

Bodin, P., K. Smith, S. Horton, and H. Hwang (2001). Microtremor observations of deep sediment resonance in metropolitan Memphis, Tennessee, *Engn. Geol.* **62,** 159–168.

Catchings, R. D. (1999). Regional Vp, Vs, Vp/Vs and Poisson's ratios across earthquake source zones from Memphis, TN, to St. Louis, MO, *Bull. Seism. Soc. Am.* **89,** 1591–1605.

Chen, K.-C., J.-M. Chiu, and Y.-T. Yang (1994). Qp–Qs relations in the sedimentary basin of the Mississippi embayment using converted phases, *Bull. Seism. Soc. Am.* **84,** 1861–1868.

Clouser, R., and C. Langston (1991). Qp–Qs relations in a sedimentary basin using converted phases, *Bull. Seism. Soc. Am.* **81,** 733–750.

Dainty, A. M. (1981). A scattering model to explain seismic Q observations in the lithosphere between 1 and 30 Hz, *Geophys. Res. Lett.* **8,** 1126–1128.

Farnbach, J. S. (1975). The complex envelope in seismic signal analysis, *Bull. Seism. Soc. Am.* **65,** 951–962.

Frankel, A., and L. Wennerberg (1987). Energy-flux model of seismic coda: separation of scattering and intrinsic attenuation, *Bull. Seism. Soc. Am.* **77,** 1223–1251.

Futterman, W. I. (1962). Dispersive body waves, *J. Geophys. Res.* **67,** 5279–5291.

Ginzberg, A., W. D. Mooney, A. W. Walter, W. J. Lutter, and J. H. Healy (1983). Deep structure of northern Mississippi embayment, *AAPG Bull.* **67,** 2031–2046.

Goldstein, P., D. Dodge, and M. Firpo (2002). SAC2000: signal processing and analysis tools for seismologists and engineers, in *IASPEI International Handbook of Earthquake and Engineering Seismology*, W. H. K. Lee, H. Kanamori, P. C. Jennings, and C. Kisslinger (Editors), Academic Press, San Diego, California.

Hashash, Y. M. A., and D. Park (2001). Non-linear one-dimensional seismic ground motion propagation in the Mississippi embayment, *Engn. Geol.* **62,** 185–206.

Johnston, A. C., and E. S. Schweig (1996). The enigma of the New Madrid earthquakes of 1811–1812, *Annu. Rev. Earth. Planet. Sci.* **24,** 339–384.

Kang, I. B., and G. McMechan (1994). Separation of intrinsic and scattering Q based on frequency-dependent amplitudes of transmitted waves, *J. Geophys. Res.* **99,** 23,875–23,885.

Kelson, K. I., G. D. Simpson, R. B. V. Arsdale, C. C. Haraden, and W. R. Lettis (1996). Multiple Holocene earthquakes along the Reelfoot fault, central New Madrid seismic zone, *J. Geophys. Res.* **202,** 6151–6170.

Langston, C. A. (2003a). Local earthquake wave propagation through Mississippi embayment sediments, part I: body wave phases and local site responses, *Bull. Seism. Soc. Am.* **93,** 2664–2684.

Langston, C. A. (2003b). Local earthquake wave propagation through Mississippi embayment sediments, part II: influence of local site velocity structure on Qp–Qs determinations, *Bull. Seism. Soc. Am.* **93,** 2685–2702.

Langston, C. A. (2004). Seismic ground motions from a bolide shock wave, *J. Geophys. Res.* **109,** B12309, doi 10.1029/2004JB003167.

Langston, C. A., W. Mooney, P. Bodin, C. Powell, and M. Withers (2002a). Experiment in New Madrid Zone to employ active source, *EOS Trans. AGU* **83,** 473.

Langston, C. A., A. A. Nyblade, and T. J. Owens (2002b). Regional wave propagation in Tanzania, East Africa, *J. Geophys. Res.* **107,** B1, doi 10.1029/2001JB000167.

Liu, Z., M. E. Wuenscher, and R. B. Herrmann (1994). Attenuation of body waves in the central New Madrid seismic zone, *Bull. Seism. Soc. Am.* **84,** 1112–1122.

Mooney, W. D., M. C. Andrews, A. Ginzburg, D. A. Peters, and R. M. Hamilton (1983). Crustal structure of the northern Mississippi embayment and a comparison with other continental rift zones, *Tectonophysics* **94,** 327–348.

Nuttli, O. W. (1973). The Mississippi Valley earthquakes of 1811 and 1812: intensities, ground motions, and magnitudes, *Bull. Seism. Soc. Am.* **63,** 227–248.

Park, D. (2003). Estimation of non-linear seismic site effects for deep deposits of the Mississippi embayment, *Ph.D. Thesis*, University of Illinois, Urbana-Champaign.

Pujol, J., S. Pezeshk, Y. Zhang, and C. Zhao (2002). Unexpected values of Qs in the unconsolidated sediments of the Mississippi embayment, *Bull. Seism. Soc. Am.* **92,** 1117–1128.

Self, R. P. (1993). Late Tertiary to early Quaternary sedimentation in the Gulf coastal plain and lower Mississippi valley, *Southeast. Geol.* **33,** 99–110.

Stearns, R. G. (1957). Cretaceous, Paleocene, and lower Eocene geologic

history of the northern Mississippi embayment, *Geol. Soc. Am. Bull.* **68,** 1077–1100.

Stearns, R. G., and M. V. Marcher (1962). Late Cretaceous and subsequent structural development of the northern Mississippi embayment area, *Geol. Soc. Am. Bull.* **73,** 1387–1394.

Tuttle, M. P., and E. S. Schweig (1999). Towards a paleoearthquake chronology for the New Madrid seismic zone, *U.S. Geol. Surv. NEHRP Ann. Rept*, 17 pp.

Tuttle, M. P., J. D. Sims, K. Dyer-Williams, I. R. H. Lafferty, and I. E. S. Schweig (2000). Dating of liquefaction features in the New Madrid seismic zone, U.S. Nuclear Regulatory Commission, 78 pp.

Vassiliou, M., C. A. Salvado, and B. R. Tittmann (1982). *Seismic Attenuation*, CRC Press, Boca Raton, Florida.

Vogfjord, K. S., and C. A. Langston (1996). Characteristics of short-period wave propagation in regions of Fennoscandia, with emphasis on Lg, *Bull. Seism. Soc. Am.* **86,** 1873–1895.

Vucetic, M. (1994). Cyclic threshold shear strains in soils, *J. Geotech. Eng.* **120,** 2208–2228.

Wang, Z., R. Street, E. Woolery, and J. Harris (1994). Qs estimation for unconsolidated sediments using first-arrival SH wave critical refractions, *J. Geophys. Res.* **99,** 13,543–13,551.

Wessel, P., and W. H. F. Smith (1998). New, improved version of Generic Mapping Tools released, *EOS Trans.* **79,** 579.

Center for Earthquake Research and Information
University of Memphis
Memphis, Tennessee 38152
(C.A.L., P.B., C.P., M.W., S.H.)

U.S. Geological Survey
Menlo Park, California
(W.M.)

Manuscript received 18 March 2005.